Available online at www.sciencedirect.com
SCIENCE DIRECT®
Journal of Nuclear Materials 337–339 (2005) 669–676
journal of nuclear materials
www.elsevier.com/locate/jnucmat

Power deposition onto plasma facing components in poloidal divertor tokamaks during type-I ELMs and disruptions

T. Eich [a,*], A. Herrmann [a], G. Pautasso [a], P. Andrew [b], N. Asakura [c], J.A. Boedo [d], Y. Corre [e], M.E. Fenstermacher [f], J.C. Fuchs [a], W. Fundamenski [b], G. Federici [g], E. Gauthier [e], B. Goncalves [h], O. Gruber [a], A. Kirk [b], A.W. Leonard [i], A. Loarte [j], G.F. Matthews [b], J. Neuhauser [a], R.A. Pitts [k], V. Riccardo [b], C. Silva [h]

[a] *Max-Planck-Institut für Plasmaphysik, IPP-EURATOM Association, Boltzmann str. 2, D-85748 Garching, Germany*
[b] *EURATOM-UKAEA Fusion Association, Culham Science Center, Abingdon, Oxon OX 14 3DB, UK*
[c] *Naka Fusion Research Establishment, JAERI, Japan*
[d] *University of California, San Diego, La Jolla, CA 92093, USA*
[e] *Association EURATOM CEA, Cadarache, 13108 St. Paul-lez-Durance, France*
[f] *Lawrence Livermore National Laboratory, Livermore, CA 94551, USA*
[g] *ITER JWS, Max-Planck-Institut für Plasmaphysik, Garching, Germany*
[h] *Associacao EURATOM/IST, Instituto Superior Tecnico, Portugal*
[i] *General Atomics, P.O. Box 85608, San Diego, CA 92186-5608, USA*
[j] *CSU-EFDA, Max-Planck-Institut für Plasmaphysik, Garching, Germany*
[k] *Association EURATOM, CRPP-EPFL, 1015 Lausanne, Switzerland*

Abstract

A comparative analysis of the spatial and temporal characteristics of transient energy loads (ELMs and disruptions) on plasma facing components (PFCs) in present tokamak devices and their extrapolation to next step devices is presented. Type I ELMs lead to the expulsion of energy by the plasma in helical structures with ballooning-like features and toroidal numbers in the range $n = 10$–15. The plasma energy is transported towards the divertor and the main chamber PFCs leading to significant transient energy loads at these two locations on small wetted area. The largest transient energy fluxes onto PFCs in tokamaks are measured during the thermal quench of disruptions. These fluxes do not exceed greatly those of large Type I ELMs, due to the much larger wetted area for energy flux during the thermal quench compared to Type I ELMs. The implications of these findings for the next step devices are discussed.

PACS: 52.55.Fa; 52.25.Vy; 52.55.Rk; 52.40.Hf
Keywords: Power deposition; Divertor; First wall; ELMs; Disruption

* Corresponding author. Tel.: +49 3834 88 1283; fax: +49 3834 88 2719.
E-mail address: thomas.eich@ipp.mpg.de (T. Eich).

0022-3115/$ - see front matter
doi:10.1016/j.jnucmat.2004.09.051

1. Introduction

Operation in H-Mode [1] is generally assumed as the reference scenario for a next step tokamak device such as ITER [2]. In an H-mode plasma a pronounced edge transport barrier with steep edge gradients is observed. These steep gradients are affected by quasi-periodic barrier relaxations named Edge Localized Modes (ELMs) [3]. Best global plasma performance is usually obtained in the type-I ELM regime with sudden releases of some tens of percent of the plasma stored energy in the pedestal region towards the scrape-off-layer (SOL). The timescales of (1) the barrier relaxation ($\tau_{\mathrm{MHD}}^{\mathrm{ELM}}$), (2) the parallel transport time (determined by the ions) along open field lines towards the divertor regions ($\tau_{\parallel}^{\mathrm{ELM}}$) and (3) the perpendicular transport ($\tau_{\perp}^{\mathrm{ELM}}$) are in the range of some hundreds of microseconds. The high resulting heat fluxes on the plasma facing components (PFC) may cause an intolerable transient thermal load for a larger device. The normalized size of the pedestal energy losses during type-I ELMs ($E_{\mathrm{ELM}}/E_{\mathrm{ped}}$) is in the range of 1–10% for ASDEX Upgrade [4], 5–30% for JET [5] and 4–30% for DIII-D [6] with $E_{\mathrm{ped}} = 3/2 \times n_{e,\mathrm{ped}} \times [T_{e,\mathrm{ped}} + T_{i,\mathrm{ped}}] \times V_{\mathrm{plasma}}$. The quantity E_{ELM} is the difference of the plasma stored energy before and after the ELM event, $n_{e,\mathrm{ped}}$ is the electron density, $T_{e,\mathrm{ped}}$ and $T_{i,\mathrm{ped}}$ are the electron and ion temperature at the pedestal top, respectively. Different approaches for scaling the pedestal energy losses during type-I ELMs give values between 5 MJ [5] and 30 MJ [7] for ITER. A formulation for quantifying the maximum acceptable energy of an ELM is given in Section 2 as well as details of the state of present understanding of the components which go into this formulation.

As the active divertor receives the largest fraction of the power crossing the separatrix, investigations have previously been focused on this area. Divertor measurements have shown that type-I ELMs can deposit as little as 50% of the plasma energy loss (E_{ELM}) onto the divertor target plates ($E_{\mathrm{ELM}}^{\mathrm{target}}$), introducing the possible problem of significant deposition on the main chamber wall and resultant thermal ablation there. A full power balance requires thermal measurements of all the first wall components as well as complementary ELM-resolved radiation measurements. The results of these experiments are summarized in Section 3.

The fast loss of the plasma energy (thermal quench) and of plasma current (current quench) due to a major disruption also pose a threat to PFCs of a next step tokamak. While the total energies involved in the two processes are similar, the thermal quench is considered to be more critical due to its order of magnitude smaller deposition time. The problem of extrapolating the power flux on PFCs during the thermal quench is similar to that of type-I ELMs as presented in Section 4.

2. Power load characteristics for the divertor target plates during type-I ELMs

For next step fusion devices such as ITER, the limit on the transient heat load due to ELMs is derived from the ablation or melting limit of the PFC. The ablation temperature for carbon is 2300 °C. Each increase of the temperature of the carbon plates above this value will lead to erosion of the target material. Accepting a restricted lifetime for the carbon divertor target plates of 10^6 ELMs (corresponding to 1000 discharges with 1000 ELMs per discharge), a tolerable temperature $T_{\mathrm{tolerable}} = 3000$ °C can be estimated [8]. Based on this number we are able to calculate the maximum tolerable temperature increase by single ELMs including also the expected stationary peak temperature of $T_{\mathrm{stationary}}^{\mathrm{outer}} = 1500$ °C for the outboard divertor and $T_{\mathrm{stationary}}^{\mathrm{inner}} = 400$ °C for the inboard divertor in ITER [7,9]. We find $\Delta T_{\mathrm{ELM}} \leqslant T_{\mathrm{tolerable}} - T_{\mathrm{stationary}}^{\mathrm{outer}} = 1500$ K and $\Delta T_{\mathrm{ELM}} \leqslant T_{\mathrm{tolerable}} - T_{\mathrm{stationary}}^{\mathrm{inner}} = 2600$ K. The value for ΔT_{ELM} corresponds to an energy $E_{\mathrm{ELM}}^{\Delta T}$ as it is given in a simple function of the thermal material properties $C_{\mathrm{mater}}^{\mathrm{thermal}}$, wetted area A_{ELM} and timescales $\tau_{\mathrm{ELM}}^{\mathrm{target}}$ of the ELM heat flux on target [10]:

$$C_{\mathrm{mater}}^{\mathrm{thermal}} \times \frac{E_{\mathrm{ELM}}^{\Delta T}}{A_{\mathrm{ELM}} \times \sqrt{\tau_{\mathrm{target}}^{\mathrm{ELM}}}} \leqslant \Delta T_{\mathrm{ELM}} = 1500\ \mathrm{K}. \tag{1}$$

To compare the maximum tolerable ELM energy ejected during an ELM event E_{ELM} to the energy contributing to the thermal load on the target $E_{\mathrm{ELM}}^{\Delta T}$ we need further to summarize our knowledge about the fraction of E_{ELM} that is deposited on the target (f_{target}), the fraction that is deposited on the outer/inner divertor ($f_{\mathrm{outer}} = 1 - f_{\mathrm{inner}}$) and the fraction of the energy ($f_{\mathrm{peak}}^{\mathrm{outer}}$ and $f_{\mathrm{peak}}^{\mathrm{inner}}$) leading to the temporal peak temperature. With this nomenclature we get, e.g. for the outboard divertor

$$E_{\mathrm{ELM}}^{\Delta T} = E_{\mathrm{ELM}} \times f_{\mathrm{target}} \times f_{\mathrm{outer}} \times f_{\mathrm{peak}}^{\mathrm{outer}}. \tag{2}$$

A comparable or even larger fraction of the ELM energy is found on the inboard divertor in current devices. The ELM outboard divertor load is still more restrictive since the outer target is heated up to 1500 °C peak temperature due to the Inter-ELM power load whereas the inner target is expected to have peak temperature of only 400 °C. For this reason we will focus mainly on the presentation of the required values from Eqs. (1) and (2) for the outboard divertor.

The fraction of the ELM energy released from the pedestal plasma (E_{ELM}) that is deposited onto the divertor target ($E_{\mathrm{ELM}}^{\mathrm{target}}$) is shown in Fig. 1 for JET MKII-GasBox and JET DOCL divertor discharges [11,12]. This fraction varies between 0.5 and 1.0 for the data from both experimental campaigns. As can be seen in the figure, larger ELMs tend to deposit a smaller fraction of

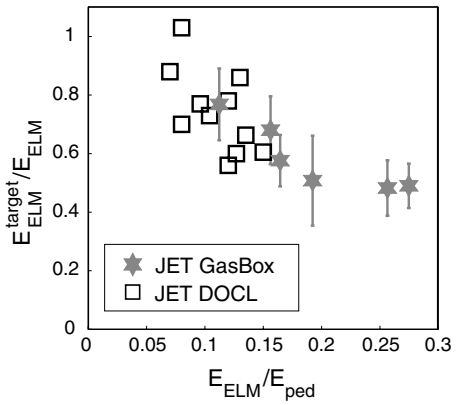

Fig. 1. The fraction of the ELM energy losses at the midplane that is deposited on the divertor target ($f_{target} = E^{target}_{ELM}/E_{ELM}$) as a function of the normalized ELM energy (E_{ELM}/E_{ped}) for JET GasBox and DOCL discharges.

the released energy into the divertor region in JET. We find an average value for $f_{target} = E_{ELM}/E^{target}_{ELM} = 0.75 \pm 0.25$. Fig. 2 shows the temporal evolution of inboard and outboard deposited power due to ELMs onto the (a) ASDEX Upgrade DIV-IIb and (b) JET MKII-SRP divertor target plates. In both cases a typical ELM is presented, which is a coherent average of 15 consecutive ELMs. The variation of the typical evolution is not yet available but should be addressed in future works. The temporal evolution of the power deposition onto both target plates in both experiments appears to be similar. The relative ELM size (E_{ELM}/E_{ped}) for JET and ASDEX Upgrade is roughly 10%. The absolute

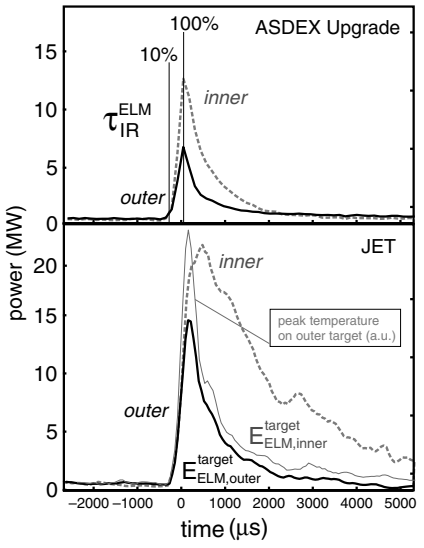

Fig. 2. Temporal evolution of the power deposition during an ELM event onto the divertor target plates in JET and ASDEX Upgrade. Temporal evolution of the peak temperature on the outer target in JET.

pedestal loss (E_{ELM}) and the deposited energy (E^{target}_{ELM}) on target is larger for JET, since the plasma stored energy for the presented case is about a factor of 3 higher.

Fig. 2 shows that the total deposited ELM energy E^{target}_{ELM} onto the inner $E^{target}_{ELM,inner}$ is larger than onto the outer divertor targets $E^{target}_{ELM,outer}$ ($E^{target}_{ELM} = E^{target}_{ELM,inner} + E^{target}_{ELM,outer}$). Note that the power release between ELMs comes dominantly from the low field side [13] and most of this power is deposited on the outboard divertor [14,15,11]. ELM energy is also released preferentially near the outer midplane consistent with the peeling-ballooning MHD characteristics for ELMs [16,17]. The mechanism that drives a higher fraction of the ELM energy towards the inner target compared to the Inter-ELM phases is not yet clear. The same observation has been made in JT-60U [18] and DIII-D [19]. Thermographic measurements from JET [11], DIII-D [19] and ASDEX Upgrade [7] have shown a fraction of the divertor deposited energy on the outer target $f_{outer} = E^{target}_{ELM,outer}/E^{target}_{ELM} = 0.4 \pm 0.2$.

The ELM energy pulse to the divertor target can be separated into two phases as illustrated in Fig. 2. In the first phase ($t \leqslant \tau^{ELM}_{IR}$) the target temperature and the power increase up to a peak value and in the second phase ($t \geqslant \tau^{ELM}_{IR}$) the target temperature decays back to the Inter-ELM value although still energy is reaching the divertor target. The time to reach the peak value for the temperature or power is found to be identical within the uncertainty of the measurements. The characteristic timescale τ^{ELM}_{IR} for the first phase is defined as the duration of the power increase from 10% above the initial value to 100% of the maximum measured value [11] and is determined as shown in Fig. 2. Only the fraction of the ELM energy (f_{peak}) that is deposited before τ^{ELM}_{IR} will lead to the maximum peak temperature on the divertor target during an ELM. This way we find $f_{peak} = E^{target}_{ELM}(t \leqslant \tau^{ELM}_{IR})/E^{target}_{ELM}$ and can identify the characteristic time scale τ^{ELM}_{target} from Eq. (1) with the experimentally quantified value τ^{ELM}_{IR} as shown in Fig. 2 to get $\tau^{ELM}_{IR} = \tau^{ELM}_{target}$. Numerical modelling of the target temperature evolution for conditions during the ELM power load in ITER came to the same conclusion [8].

Fig. 3 shows the dependence of f^{outer}_{peak} on τ^{ELM}_{IR} for the outboard divertor target in JET DOCL discharges [12]. The fraction of the ELM energy deposited during the power rise phase stays below 45% and can be as low as 20% for smaller τ^{ELM}_{IR}. This finding indicates that there is a correlation between the dominant parallel energy transport mechanism towards the divertor along field lines and the fraction of energy deposited in the first phase of the ELM target heat fluxes [12]. Experimentally a value of $f^{outer}_{peak} = 0.32 \pm 0.08$ is observed but further work is required to improving the database. The estimation of the power pulse shape on the divertor by infrared measurements is affected by co-deposited

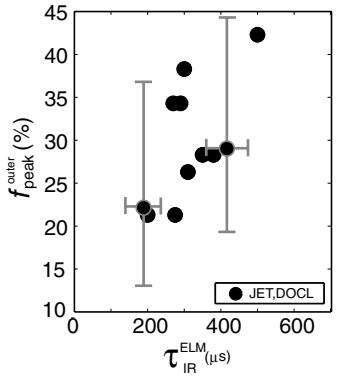

Fig. 3. The fraction $f_{\text{peak}}^{\text{outer}} = E_{\text{ELM}}^{\text{target}}(t \leqslant \tau_{\text{IR}}^{\text{ELM}})/E_{\text{ELM}}^{\text{target}}$ varies between values of 20% and 45% for the outboard divertor in JET DOCL discharges.

surface layers [20] and surface inhomogenities on micron spatial scales [21]. Layers have been dominantly observed on the inner divertor in JET, which is identified as the dominant deposition zone for standard field directions [22]. Surface layers are reported to have less influence on the outboard divertor target since this is a net erosion zone. A corresponding value for $f_{\text{peak}}^{\text{inner}}$ for the inboard divertor heat load has not been quantified.

The timescale $\tau_{\text{IR}}^{\text{ELM}}$ of the power deposition on the divertor target is correlated with the collisionless flight time of the pedestal energy ions to the divertor $\tau_{\parallel}^{\text{ELM}}$ as shown in Fig. 4 [7,23,19]. The value $\tau_{\parallel}^{\text{ELM}}$ is defined as $\tau_{\parallel}^{\text{ELM}} = 2\pi q_{95} \times R_{q_{95}}/\sqrt{(T_e + T_i)/m_d}$, assuming $T_e = T_i = T_{\text{ped}}$ and m_d is the mass of the deuterium ions. Note that $\tau_{\parallel}^{\text{ELM}}$ contains only the pedestal top electron temperature and a characteristic length. The good correlation of $\tau_{\parallel}^{\text{ELM}}$ with $\tau_{\text{IR}}^{\text{ELM}}$ is in agreement with PIC-simulations [24] suggesting convective transport along open field lines during type-I ELMs towards the divertor target.

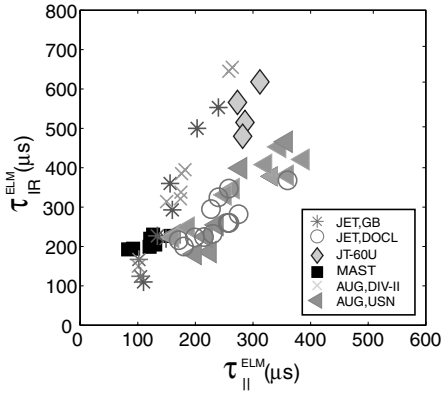

Fig. 4. The characteristic timescale $\tau_{\text{IR}}^{\text{ELM}}$ of the power deposition on the divertor target plate as a function of $\tau_{\parallel}^{\text{ELM}}$ for JET GasBox (GB), JET diagnostic optimized configuration (DOCL), JT-60U, MAST and ASDEX Upgrade Divertor-II (DIV-II) and Upper Single Null (USN) discharges.

In ELM resolved probe studies in TCV [25], JET [26], ASDEX Upgrade [14], MAST [27] and DIII-D [19], a delay in the response of the divertor plasma to pedestal energy ions relative to pedestal energy electrons was observed as expected for a convective transport of energy. Studies of the soft X-ray emission from the divertor target surfaces during the start phase of ELMs in JET suggest bremsstrahlung emission caused by fast electrons, consistent with the idea that these electron losses would then lead to a sheath potential restricting further losses to the ion loss time [28]. However, the concept of a characteristic length $L = 2\pi q_{95} R_{q_{95}}$ may be oversimplified as eventually the ELM related magnetic perturbation will directly connect field lines from the pedestal with the targets [6,29].

A characterization of the ELM pedestal losses separately in temperature and density has revealed both conductive (ΔT_e) as well as convective (Δn_e) ELM losses for DIII-D [6], JET [5] and ASDEX Upgrade [4]. An extended comparison of conductive/convective pedestal losses with transport times including the systematic variation of the relation between $\tau_{\text{IR}}^{\text{ELM}}$ and $\tau_{\parallel}^{\text{ELM}}$ as observed for various divertor geometries remains to be done. Based on the expected pedestal temperatures for ITER, one estimates a $\tau_{\parallel}^{\text{ELM}} = 234$ μs [5]. From Fig. 4, the corresponding estimate of $\tau_{\text{IR}}^{\text{ELM}}$ for ITER is then 400 μs ± 150 μs.

In addition to the parallel transport timescale, one has to take into account the timescales of the MHD processes which lead to the energy losses ($\tau_{\text{MHD}}^{\text{ELM}}$). In MAST the value found experimentally by probe measurements [27] is $\tau_{\text{MHD}}^{\text{ELM}} \approx 87$ μs. This value agrees with the energy loss timescale caused by an explosive finger-like instability, which is described by non-linear MHD ballooning calculation $\tau_{\text{MHD}}^{\text{ELM}} \approx \tau_{\text{MHD}}^{\text{explosive}} = (\tau_{\text{A}}^2 \tau_{\text{E}})^{1/3}$ where τ_{A} is the shear Alfvén time and τ_{E} is the global energy confinement time [30].

An important quantity to describe the expected target heat load for a larger device is the radial target decay length. As shown in [31], ELM profiles on the target display a steep power fall off near the separatix (λ_{ELM}) and a longer fall off length remote from the strike point, which does not play a role for the divertor load. The fall off length near the separatrix (λ_{ELM}) was compared to the between ELM fall off length ($\lambda_{\text{Inter-ELM}}$) for JET, ASDEX Upgrade [14], DIII-D [32] and JT-60U [18]. In all experiments a mean value for $\lambda_{\text{ELM}}/\lambda_{\text{Inter-ELM}} = 1$–1.5 is reported. In this paper we will therefore assume an ELM wetted area $A_{\text{ELM}} = A_{\text{stationary}} \times (1.25 \pm 0.25)$ and we use for ITER $A_{\text{stationary}} \approx 3\ \text{m}^2$ from [23]. So far no correlation of λ_{ELM} with the normalized ELM energy has been reported.

Recent target heat load measurements from ASDEX Upgrade [29] have confirmed earlier suggestions [33,31] that the ELM energy ejection is toroidally asymmetric in the midplane. In addition to the usual axisymmetric

strike point line, non-axisymmetric and slightly inclined stripes are observed in the remote region radially outwards from the strike point line. Multiple peak structures in ELM heat flux profiles have also been reported in JT-60U [18] and JET [34]. The non-axisymmetric stripes are smeared out to a toroidally symmetric power deposition pattern on the target at the strike lines. The heat flux pattern is consistent with toroidal mode numbers of around 10–15; this value is also found by H_α visible light measurements both in MAST [35] as well as in JET [36]. The largest fraction of energy which is deposited on target during ELMs is measured close to the strike line, so no large toroidal peaking factor is expected for the maximum heat flux and for the (spatially integrated) target deposited power. The estimated toroidal peaking factor for the ELM power measured at two toroidal locations in DIII-D of less than 1.5 is consistent with this [32].

Based on the findings above, we can combine Eqs. (1) and (2) to calculate the maximum tolerable ELM energy $E_{\mathrm{ELM}}^{\mathrm{ITER}}$ for the ITER outboard divertor as

$$C_{\mathrm{mater}}^{\mathrm{thermal}} \times \frac{E_{\mathrm{ELM}}^{\mathrm{ITER}} \times f_{\mathrm{target}} \times f_{\mathrm{outer}} \times f_{\mathrm{peak}}^{\mathrm{outer}} \times \frac{3}{2}}{A_{\mathrm{ELM}} \times \sqrt{\tau_{\mathrm{IR}}^{\mathrm{ELM}}}} \leqslant 1500\ \mathrm{K}, \tag{3}$$

$$E_{\mathrm{ELM}}^{\mathrm{ITER}} \leqslant \frac{2}{3} \times \frac{1500\ \mathrm{K}}{C_{\mathrm{mater}}^{\mathrm{thermal}}} \times \frac{A_{\mathrm{ELM}} \times \sqrt{\tau_{\mathrm{IR}}^{\mathrm{ELM}}}}{f_{\mathrm{target}} \times f_{\mathrm{outer}} \times f_{\mathrm{peak}}^{\mathrm{outer}}}. \tag{4}$$

We use the values presented in the previous sections of $\tau_{\mathrm{IR}}^{\mathrm{ELM}} = 400\ \mu\mathrm{s} \pm 150\ \mu\mathrm{s}$, $f_{\mathrm{target}} = 0.75 \pm 0.25$, $f_{\mathrm{outer}} = 0.4 \pm 0.2$ and $f_{\mathrm{peak}}^{\mathrm{outer}} = 0.32 \pm 0.08$. For the outer target in ITER, $A_{\mathrm{ELM}} = 3.75 \pm 0.75\ \mathrm{m}^2$, and using the thermal material properties of the ITER carbon tiles gives $E_{\mathrm{ELM}}^{\mathrm{ITER}} \leqslant 11.1\ \mathrm{MJ} \pm 7\ \mathrm{MJ}$ per ELM. The factor 3/2 in Eq. (3) takes into account the temporal evolution of the power deposition that is approximated to be constantly increasing for $t \leqslant \tau_{\mathrm{IR}}^{\mathrm{ELM}}$; a constant power deposition for $t \leqslant \tau_{\mathrm{IR}}^{\mathrm{ELM}}$ would give a factor of 1. The uncertainty in $E_{\mathrm{ELM}}^{\mathrm{ITER}}$ is calculated by assuming independent Gaussian distributions for each individual value. A detailed analysis of the distribution of single values and their covariance remains for future analysis; this could be an important extension since infrequent, large ELMs potentially reduce the divertor lifetime more than the most frequent ELMs [8]. The same formalism gives a value of around $E_{\mathrm{ELM}}^{\mathrm{ITER}} \leqslant 36.6\ \mathrm{MJ} \pm 19\ \mathrm{MJ}$ for the inboard divertor assuming $f_{\mathrm{peak}}^{\mathrm{inner}} = f_{\mathrm{peak}}^{\mathrm{outer}}$.

3. Power load outside the divertor during type-I ELMs

The largest fraction of radiation due to the ELM is found in the inner divertor. Here a fraction between 10% and 40% of the plasma energy loss (E_{ELM}) is reported to be radiated ($E_{\mathrm{ELM}}^{\mathrm{rad}}$) in ASDEX Upgrade [37]. The ELM radiation fraction $E_{\mathrm{ELM}}^{\mathrm{rad}}/E_{\mathrm{ELM}}$ decreases with increasing normalized ELM energy $E_{\mathrm{ELM}}/E_{\mathrm{ped}}$. The temporal evolution of the radiation during single type-I ELMs can not be resolved due to the limited (1 ms) time resolution of the bolometers. Balancing the ELM loss energy (E_{ELM}) with the radiated ELM energy ($E_{\mathrm{ELM}}^{\mathrm{rad}}$) and ELM energy to the active divertor target plates ($E_{\mathrm{ELM}}^{\mathrm{target}} = E_{\mathrm{ELM,outer}}^{\mathrm{target}} + E_{\mathrm{ELM,inner}}^{\mathrm{target}}$) in ASDEX Upgrade, a fraction of missing energy of around 5–10% is found when averaging many ELMs in discharges with low average input power. A larger fraction of missing energy of around 15–25% is estimated for shots with larger $E_{\mathrm{ELM}}/E_{\mathrm{ped}}$, experimentally achieved by increasing the triangularity and the input power in this case. The experimental decrease of $E_{\mathrm{ELM}}^{\mathrm{rad}}/E_{\mathrm{ELM}}$ with increasing $E_{\mathrm{ELM}}/E_{\mathrm{ped}}$ is consistent with modeling that shows negligible ELM radiation fraction in ITER for large type-I ELMs [38]. Detailed studies of the feasibility of dissipating the ELM energy in the SOL by impurity seeding techniques in JET have shown that higher impurity content does not increase the $E_{\mathrm{ELM}}^{\mathrm{rad}}/E_{\mathrm{ELM}}$ except in the case of extremely small ELMs [39–41].

To quantify the thermal load on the first wall in ASDEX Upgrade, a fast 2D thermography system was brought into operation to measure the power load on parts of the outer wall limiters, antenna limiters and inner heat shield [42]. The power deposition due to ELMs is found to be in the same range as the far SOL divertor target heat fluxes when expressed as parallel heat fluxes. Individual ELMs impose in their start phase ($t \leqslant \tau_{\mathrm{IR}}^{\mathrm{ELM}}$) a localized heat flux deposition pattern on the limiters radially closest to the outer midplane. The average heat fluxes from many ELMs result in a poloidally homogenous temperature pattern on the limiters suggesting that the localized heat fluxes are poloidally varying when hitting the toroidally localized limiters. No significant localized power deposition has been found on the inner heat shield in ASDEX Upgrade. The normalized radial ELM transport energy across the SOL onto the first wall ($E_{\mathrm{ELM}}^{\mathrm{wall}}/E_{\mathrm{ELM}}$) is around 15%. In that respect it is interesting to note that $E_{\mathrm{ELM}}^{\mathrm{wall}} = 1.5 \times E_{\mathrm{Inter\text{-}ELM}}^{\mathrm{wall}}$ whereas for the divertor usually $E_{\mathrm{ELM}}^{\mathrm{divertor}} = 0.3 \times E_{\mathrm{Inter\text{-}ELM}}^{\mathrm{divertor}}$ is found; ELMs carry the dominant fraction of the energy transported to the outer wall.

The ELM multiple peak structure observed, e.g., on the divertor target in ASDEX Upgrade corresponds to helical flux bundles in the outer midplane region [29]. These helical flux bundles are observed in MAST first to balloon out beyond the separatrix, then to detach and finally to move radially outwards as filaments until hitting the wall [35]. These filaments are also reflected in a poloidal substructure as observed by poloidally resolving fluctuation diagnostics in ASDEX and JET [43,44]. From the current analysis it is not clear which fraction of E_{ELM} is lost along open field lines during the

detachment process and which fraction of E_{ELM} is in the filaments. The midplane temperature and density decay lengths of these filaments once they are moving radially across the SOL have been measured in DIII-D [45] as presented in Fig. 5. In the high-density discharge with small ELMs a small radial density decay length is observed. In the low-density discharge with larger ELMs a larger radial density decay length is estimated. The temperature decay length as shown in Fig. 5 is not clearly correlated to the ELM energy or density. From DIII-D it is also reported that the radial propagation of the filaments peaks at 500 m/s and decays to 120 m/s propagating 6–7 cm in the SOL and corresponding to a perpendicular transit time of 200 μs [45]. The carbon ion temperature during the ELM cycle has been measured directly in DIII-D and revealed that the temperature of the radially transported carbon ions during the ELM in the SOL is similar to the pre-ELM pedestal carbon ion temperature [46].

Reciprocating probe (RCP) measurements at JET [43,47] show that an effective radial drift velocity during the ELM is proportional to ELM size as presented in Fig. 6. The effective velocity is a temporal average over the whole ELM duration (multiple filaments are included in the average) and in the range of 50–150 m/s. Peak values of up to 1000 m/s for single filaments are measured. The RCP was located 4 cm from the LCFS when mapped to the outer midplane. Another study of

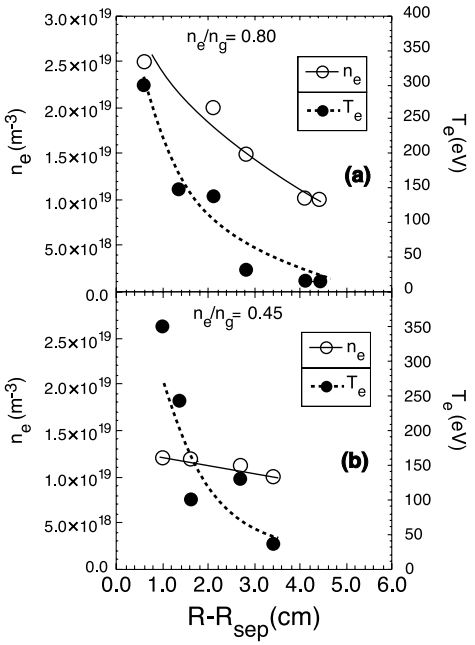

Fig. 5. Density and electron temperature profiles of ELM filaments measured by reciprocating probe in DIII-D for two different line averaged densities: (a) high density (small ELMs) and (b) low density (large ELMs).

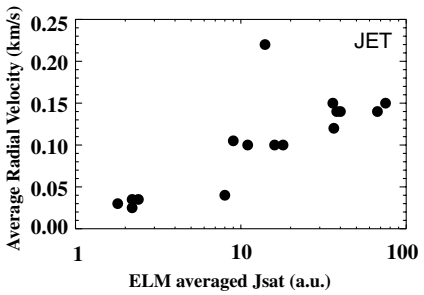

Fig. 6. The radial velocity of the observed ELM filaments increases with the ELM averaged j_{sat} as demonstrated by RCP probe measurements for JET; j_{sat} is expected to scale roughly proportionally to the normalized ELM energy.

ELM characteristics was made using an array of Langmuir probes (LP) mounted at the outer wall limiters at JET with distances of 0.1–0.2 m to the LCFS [15]. These probes derive a radial transport velocity in the range of 450 m/s by measuring the arrival time differences for single ELMs to the various LPs. Furthermore, an electron temperature of 25–30 eV at the outer wall limiters is indicated by the LP data. Based on the assumption that the ELM related transport across the SOL is described by a sheath limited plasma-blob [48], the related decay lengths can be inferred and values for $\lambda_{T_e} = 3$ cm, $\lambda_{T_i} = 8$ cm and a $\lambda_{n_e} = 12$ cm are estimated [15]. These findings imply a much higher temperature of some hundreds of eV for the ions arriving at the limiters, which could explain the large ELM power load there [15]. The reported values for JET correspond to the low density DIII-D case shown in Fig. 5.

Combining these observation with the findings about the divertor target heat fluxes, a qualitative picture arises. Larger ELMs consist of larger single filaments which travel faster radially across the SOL towards the outer wall limiters. Since $\tau_{\parallel}^{ELM}$ and the $\tau_{\perp}^{ELM}$ are similar, a higher radial velocity across field lines results in a lower fraction of the ELM energy from the filaments that is transported parallel along field lines towards the divertor target plates for larger ELMs.

4. Heat fluxes during disruptions

The striking signatures of a disruption are the fast loss of the plasma thermal energy (thermal quench) and the decay of the plasma current (current quench), thus terminating the plasma discharge. In the thermal quench most of the plasma thermal energy is deposited by conduction and/or convection on the limiter and divertor surfaces. Its duration depends strongly on the machine size; it is of the order of tens of microseconds in small tokamaks and hundreds of microseconds in JET. The extrapolation of the thermal quench time to an ITER plasma is 1 ms [2]. The energy flux onto the PFCs

during the thermal quench (mostly transfer of plasma thermal energy to the PFCs) is believed to be more critical than the flux during the current quench, which is mostly transfer of the magnetic energy to the PFCs in an ITER-like machine. In fact, while in ITER the plasma thermal energy of 350 MJ is comparable to the magnetic energy of 370 MJ (associated with the plasma current), the current quench duration is expected to be one order of magnitude larger than the thermal quench time [49]. The problem of extrapolating the power flux onto PFCs during the thermal quench is similar to the ELM case. Therefore this paper focuses on the energy content of a pre-disruptive plasma, the duration of the thermal quench and the broadening of the SOL during thermal quench.

The energy content of the pre-disruptive plasma compared to the energy content at full performance varies between 10% and 100% depending essentially on the disruption type. In recent studies at JET, 129 discharges were analysed, all with energies larger than 4 MJ at full performance [50]. The vast majority of the discharges reach the thermal quench with less than half of the full performance thermal energy; those reaching the thermal quench with 100% thermal energy typically have Internal Transport Barriers (20 out of 23 events).

The power deposition evolution and characteristic time of the thermal quench τ_{IR}^{tq} is observed to be similar to the τ_{IR}^{ELM} of ELMs. Typically times to reach the maximum heat flux of some hundred microseconds are observed. Similar to ELMs, the fraction of the thermal quench deposited energy that contributes to the rise in temperature at the target plates is $\leqslant$50% in ASDEX Upgrade; more precise values have to be estimated in future. Commonly a large broadening of the SOL by a factor of $\geqslant$3–5 is observed during the thermal quench in ASDEX Upgrade [51,52] and JET [53].

For many cases in ASDEX Upgrade more than 100% of the thermal quench energy E_{tq} is found as energy deposited onto the divertor plates E_{tq}^{div}. Radiation in the thermal quench E_{tq}^{rad} amounts to $\approx$50% of the thermal quench energy [51]. This finding suggests that roughly 10% of the magnetic energy (E_{mag}) must be included to fulfill the power balance leading to $E_{tq}^{div} + E_{tq}^{rad} \approx E_{tq} + 0.1 \times E_{mag}$. The value for E_{tq}^{rad} is comparable to radiation measurements in DIII-D during the thermal quench [54]. In contrast, in JET $\leqslant$50% of the thermal quench energy is found as energy deposited onto the divertor target plates, and in extreme cases only 10%. Furthermore, no large fraction of radiated power during the thermal quench is seen [55]. This implies for JET that there is a large unaccounted energy loss, presumably to the walls [49].

Based on these details from the power deposition during the thermal quench of disruptions, we consider an estimate of the maximum plasma thermal energy content at the time of the disruption that is compatible with avoiding significant ablation/melting of the PFCs in the divertor. We use for the wetted area during the thermal quench power load $A_{tq} = 3\text{–}5 \times A_{stationary}$. For the fractions necessary to compare the ejected and deposited energy as motivated in Eq. (2) for ELMs we use $f_{target}^{tq} = 0.1\text{–}1$, $f_{peak}^{tq} = 0.32$ (assumed to be identical to f_{peak} during ELMs) and $f_{outer} = f_{inner} = 0.5$. With $\tau_{target}^{tq} = \tau_{tq} = 1$ ms and otherwise the same assumptions as in Eq. (4) this gives a maximum tolerable thermal quench energy for ITER of $E_{tq}^{ITER} = 33.7\text{–}337$ MJ. A more accurate estimation depends critically on a better database for f_{target}^{tq}. This range corresponds to disruptions reaching the thermal quench at 9.6–96% of the full performance thermal energy (350 MJ) in ITER. Therefore a reliable knowledge of the power deposition details on the divertor target is absolutely essential to assess which operational range and plasma scenarios can be tolerated in ITER. Particularly in the light of the presented cross-field transport studies on ELMs, the investigations on the power load during disruptions have to be extended towards the wall. Finally it should be noted that the power deposition details could themselves depend on the disruption type. A disruption in ITER is very likely to produce ablation or melting unless some mitigation is carried out.

In DIII-D it has been demonstrated that fast noble gas injection can fully mitigate the thermal power load impact [56]. The full plasma energy in the thermal quench is radiated as the consequence of the large amount of injected noble gas. The time duration of radiation pulse is reported to be less than 1 ms, consistent with the duration of an unmitigated disruption. The radiated thermal load on the ITER wall can be estimated by dividing the plasma thermal energy of 350 MJ by the inner wall surface of 700 m^2 and the duration of less than 1 ms. The resulting thermal load of more than 500 MW/m^2 can lead to a significant melting of Be armour materials (several tens of micrometers). It is not clear at present what the effective erosion will be as a consequence of the melting process [57].

5. Conclusions

The power fluxes to the divertor target during type-I ELMs have been experimentally measured in all tokamak research groups. The results indicate that the critical fraction of the ELM pedestal loss energy will be deposited in the divertor region close to the strike line on a wetted area similar to the stationary wetted area in an expected time of some hundreds of microseconds. The maximum tolerable value for E_{ELM}^{ITER} of 11.1 MJ is within the expected range from an optimistic extrapolation of the ELM energy to ITER [5] but largely exceeded when compared to the extrapolation discussed in [14]. Different strategies, which are reviewed in [58], are proposed to mitigate the impact of single ELMs.

The ELM power load outside the divertor onto the first wall elements on the low field side is found to have values comparable to the parallel heat fluxes in the far wing of the divertor profiles. The assessment of possible material ablation due to these heat fluxes will largely depend on the ITER design for the outboard wall limiter [42]. However, from the estimated maximum tolerable energy of ELMs set by the divertor load, it is clear that only small type-I ELMs can be tolerated. These ELMs are expected to have mainly convective transport properties [5,6] and to transport most of their energy towards the divertor. From the analysis for the ITER PFC in [8] it appears that the variation from one ELM to another can have a major impact on the first wall, since the toroidally structured filaments are not smeared out as in the case for the divertor thermal load close to the strike line.

Additionally to ELMs, disruptions impose a threat for the divertor target and potentially for the first wall materials. A better quantification of the power load details, and particularly their dependence on the disruption type, must experimentally be addressed to estimate more accurate values of tolerable energies deposited during the thermal quench. Based on such an estimation, the operational space for ITER concerning the disruptivity can be judged. A powerful mitigation technique has been demonstrated which results in a complete radiation of the plasma energy homogeneously towards the walls. Nevertheless, the very short timescale of resulting radiation pulse could still introduce significant wall erosion. Future experiments are planned to improve both the data base of the thermal quench duration and its relation to τ_{IR}^{tq} as well as of the measurements of the first wall power load during disruptions.

References

[1] F. Wagner et al., Phys. Rev. Lett. 49 (1982) 1408.
[2] ITER Physics Expert Group, Nucl. Fusion 39 (1999) 2137.
[3] H. Zohm, Plas. Phys. Contr. Fusion 38 (1996) 105.
[4] H. Urano et al., Plas. Phys. Contr. Fusion 45 (2003) 1571.
[5] A. Loarte et al., Plas. Phys. Contr. Fusion 45 (2003) 1549.
[6] A. Leonard et al., Plas. Phys. Contr. Fusion 44 (2002) 945.
[7] A. Herrmann et al., J. Nucl. Mater. 313–316 (2003) 759.
[8] G. Federici et al., Plas. Phys. Contr. Fusion 45 (2003) 1523.
[9] W. Fundamenski et al., J. Nucl. Mater. 313–316 (2003) 787.
[10] G. Federici et al., J. Nucl. Mater. 313–316 (2003) 11.
[11] T. Eich et al., J. Nucl. Mater. 313–316 (2003) 919.
[12] A. Loarte et al., Phys. Plasmas 11 (2004) 2668.
[13] N. Asakura, these Proceedings. doi:10.1016/j.jnucmat.2004.10.164.
[14] A. Herrmann et al., Plas. Phys. Contr. Fusion 44 (2002) 883.
[15] W. Fundamenski et al., Plas. Phys. Contr. Fusion 46 (2004) 233.
[16] P. Snyder, H. Wilson, Contrib. Plasma Phys. 42 (2002) 258.
[17] H. Wilson et al., Phys. Plasmas 9 (2002) 1277.
[18] K. Itami et al., J. Nucl. Mater. 220–222 (1995) 203.
[19] M. Fenstermacher et al., Plas. Phys. Contr. Fusion 45 (2003) 1597.
[20] P. Andrew et al., J. Nucl. Mater. 313–316 (2003) 135.
[21] A. Herrmann et al., Phys. Scripta 111 (2004) 98.
[22] P. Andrew, these Proceedings. doi:10.1016/j.jnucmat.2004.10.145.
[23] A. Loarte et al., J. Nucl. Mater. 313–316 (2003) 962.
[24] A. Bergmann, Nucl. Fusion 42 (2002) 1162.
[25] R. Pitts et al., Nucl. Fusion 43 (2003) 1145.
[26] S. Jachmich et al., in: 28th EPS Conference on Controlled Fusion, 2001, Maderia, Portugal.
[27] A. Kirk et al., Plas. Phys. Contr. Fusion 46 (2004) 551.
[28] A. Loarte et al., Plas. Phys. Contr. Fusion 44 (2002) 1815.
[29] T. Eich, A. Herrmann, J. Neuhauser, Phys. Rev. Lett. 91 (2003) 195003.
[30] S. Cowley et al., Plas. Phys. Contr. Fusion 45 (2003) A31.
[31] D. Hill et al., J. Nucl. Mater. 241–243 (1997) 182.
[32] A. Leonard et al., J. Nucl. Mater. 241–243 (1997) 628.
[33] T. Evans, J. Nucl. Mater. 220–222 (1995) 235.
[34] E. Solano et al., these Proceedings. doi:10.1016/j.jnucmat.2004.09.067.
[35] A. Kirk et al., Phys. Rev. Lett. 92 (2004) 245002.
[36] P. Ghendrih et al., J. Nucl. Mater. 313–316 (2003) 914.
[37] C. Fuchs et al., these Proceedings. doi:10.1016/j.jnucmat.2004.09.054.
[38] A. Loarte et al., in: IAEA Fusion Energy Conference, Sorrento, Italy, 2000.
[39] J. Rapp et al., Nucl. Fusion 44 (2004) 312.
[40] G. Matthews et al., Nucl. Fusion (2003) 999.
[41] P. Monier-Garbet et al., in: 30th EPS Conference on Controlled Fusion, 2003, St. Petersburg, Russia.
[42] A. Herrmann et al., Plas. Phys. Contr. Fusion 46 (2004) 971.
[43] B. Goncalves et al., Plas. Phys. Contr. Fusion 45 (2003) 1627.
[44] M. Endler et al., Plas. Phys. Contr. Fusion, submitted for publication.
[45] J. Boedo et al., these Proceedings. doi:10.1016/j.jnucmat.2004.10.159.
[46] M. Wade et al., these Proceedings. doi:10.1016/j.jnucmat.2004.10.121.
[47] C. Silva et al., these Proceedings. doi:10.1016/j.jnucmat.2004.10.106 and doi:10.1016/j.jnucmat.2004.09.052.
[48] S. Krasheninnikov, Phys. Lett. A 283 (2001) 368.
[49] J. Paley et al., these Proceedings. doi:10.1016/j.jnucmat.2004.10.097.
[50] V. Riccardo et al., Plas. Phys. Contr. Fusion, submitted for publication.
[51] G. Pautasso et al., in: 30th EPS Conference on Controlled Fusion, 2003, St. Petersburg, Russia.
[52] G. Pautasso et al., in: 31st EPS Conference on Controlled Fusion, 2004, London, UK.
[53] V. Riccardo et al., Plas. Phys. Contr. Fusion 45 (2003) A269.
[54] E. Hollmann et al., Phys. Plasmas 10 (2003) 2863.
[55] P. Andrew et al., in: 30th EPS Conference on Controlled Fusion, 2003, St. Petersburg, Russia.
[56] D. Whyte et al., J. Nucl. Mater. 313–316 (2003) 1239.
[57] A. Loarte et al., these Proceedings. doi:10.1016/j.jnucmat.2004.09.038.
[58] M. Becoulet, these Proceedings. doi:10.1016/j.jnucmat.2004.09.074.